Improvement of the layer-layer adhesion in FFF 3D printed PEEK/carbon fibre composites

Improvement of the layer-layer adhesion in FFF 3D printed PEEK/carbon fibre composites

K. Rodzeń*[,1], E. Harkin-Jones*[,1], M. Wegrzyn[1], P. K. Sharma[1], A. Zhigunov[2]

[1] School of Engineering, Ulster University Shore Rd, Newtownabbey BT37 0QB

[2] Institute of Macromolecular Chemistry AS CR Heyrovského nám. 2, 162 00 Praha 6-Břevnov, Czechia

*corresponding author's email: kp.rodzen@ulster.ac.uk, e.harkin-jones@ulster.ac.uk

Abstract: Improvement of the mechanical properties of FFF 3D printed CF/PEEK composites was achieved by printing under favorable crystallization conditions. It was possible to improve the layer-layer tensile strength more than fivefold from 6.96 MPa to 36.28 MPa by printing in a specially customised, low cost printer operated with a heated print chamber at 230℃. The influence of the chamber temperature on the mechanical and crystalline structure was investigated to determine the best conditions. A maximum flexural modulus of 14 946 MPa and flexural stress at break of 248.9 MPa were achieved. A proof of concept study involved the 3DP of a CF/PEEK mould tooling insert for injection moulding. This insert replaced a costly traditional metal insert to print short production runs of ABS and HIPS polymers. This work offers a low cost and rapid means to produce effective tooling inserts for the injection moulding industry.

Keywords: Polymer-matrix composites (PMCs), High-temperature properties, Carbon fibres, 3-D Printing

1. Introduction

The Additive Manufacturing (AM) of thermoplastic polymers is a rapidly growing branch of polymer processing, which, with the assistance of Computer-Aided Design (CAD) software, gives unmatched freedom in product design [1]. Two common methods are used for 3D printing (3DP) of thermoplastic materials and their composites: Selective Laser Sintering (SLS) and Fused Filament Fabrication (FFF), also known as Fused Deposition Modelling (FDM) [2,3].

A key limitation of 3D printing has been the small number of engineering polymers that can be successfully printed. Limitations include printing machines that are not capable of the high temperatures and accurate temperature control needed for successfully printing such materials and also the poor Z direction strength or layer-to-layer adhesion in printed parts. Current interest from sectors such as aerospace is focused on advanced materials such as the PAEK family (polyaryletherketone) or PEI (Polyetherimide) and their composites. PAEK semicrystalline materials with their high strength to weight ratio are particularly interesting for aerospace as they have the potential to replace heavier materials such as steel or aluminum. Moreover, their self-lubricating properties, wide thermal stability windows as well as recyclability and biocompatibility are also of benefit in the automotive and medical sectors.

SLS has been successfully used for manufacturing a 3D printed PEEK (polyetheretherketone) prosthesis to replace a damaged scapula [4]. SLS was also used to print parts to investigate the mechanical performance of PEEK cranial implants made in different print orientations. There was a difference of over 300% in the failure load values for specimens printed in a horizontal alignment compared with those printed in a vertical alignment thus clearly indicating the high anisotropy of the SLS technique [5,6].

Anisotropy is also present in FFF 3DP parts due to poor layer-to-layer adhesion. For example, a tensile specimen printed horizontally as a flat tensile bar had a strength of 98.9 MPa whereas when it was printed in the Z direction its tensile strength dropped to 19.6 MPa [7]. The anisotropy in FFF reduces the applicability of the printed parts because the weakest direction determines the performance of the printed part. Thus, techniques to improve the layer-to-layer adhesion of FFF parts require investigation.

In FFF 3DP the mechanical and thermal properties of CF/PEEK composites are affected by the system of coarse pores at the layers' interface, the system of fine pores at the passes' interface and a third type of imperfection is lack of fibre impregnation. The first two are related to the thermally unfavorable conditions during printing at relatively low temperatures (typically at a building plate temperature of 95℃) which can lead to the generation of microcracks releasing the stress caused by shrinking of the material and voids. Whereas lack of impregnation of composites reinforced with continuous fibre can occur due to the short contact period between melted polymer and fibre in the extruder and nozzle during printing [8,9]. In addition to the imperfections in a 3DP structure due to poor layer-to-layer adhesion or the presence of voids, it is necessary to consider that at a fast cooling rate (e.g. when the deposited filament meets a cooler filament that has already been laid down) the crystalline phase at the interface may not be properly formed. A low degree of crystallinity will reduce the mechanical and thermal performance of the printed PEEK part. Additionally, during printing with fibre based thermoplastic composites the printing head will arrange fibres in the “XY” plane resulting in even higher anisotropy.

PEEK crystallinity can be increased by post-processing of the 3DP object. DSC studies on annealing of PEEK between T_g (143℃) and T_m (343℃) showed that it is possible to tune not only the crystallinity fraction but also the PEEK heat distortion temperature [10,11]. This points to the

potential benefits of printing with a higher chamber temperature in terms of improving mechanical performance of the printed part. It was proven that increasing the nozzle temperature from 380℃ to 420℃ at ambient chamber temperature produced an increase of the part crystallinity from 16% to 20% and increased tensile strength from 49 MPa to 59 MPa [12]. Changing the chamber temperature from 25℃ to 200℃ resulted in an increase in crystallinity from 17% to 31% and tensile strength from 58 MPa to 84 MPa. According to Yang et. al. [12], at 100℃, the crystallinity reaches around 29% and there is no significant increase in the crystallinity when chamber temperature is higher. However, the elastic modulus values at 100℃, 150℃ and 200℃ are respectively 3.3 GPa, 3.9 GPa and 4.2 GPa. This suggests the possibility of tuning the microstructure by varying the amount of energy in the form of the heat delivered to the printed part. It also suggests that not only does the level of crystallinity matter but also the thermal character of the crystalline domains.

A study of the kinetics of PEEK crystallization showed that crystallization half-time depends on temperature and is fastest around 230℃ [11]. At elevated temperatures, crystallization is controlled by nucleation whereas at low temperature it is controlled by a slow diffusion process [10]. It was noted also that PEEK possesses double melting behavior. The primary crystal melting peak has a stable position around 343℃ and is characterized by a strong, thick, well defined lamellar structure whereas a secondary melting peak can appear between T_g and T_m. The melting point of secondary crystallites depends on the temperature of annealing and is attributed to the melting of thinner and weaker lamellae. Upon heating, secondary crystallites are melted into the metastable melt and have the potential of crystallizing into new, thicker lamellar structures only if there enough time to reorganize [10,13]. A study of the influence of primary and secondary

crystalline structure on the thermal and mechanical properties of CF/PEEK is one of the aims of this study.

The mechanical performance of a 3DP object also depends on printing parameters such as infill ratio with properties decreasing as the ratio decreases [6]. The layer thickness and infill architecture also play a significant role [14,15]. An extensive study of the effect of raster orientations of 0º, 90º and alternating 0º/90º on the tensile strength of a PEEK composite showed that the highest tensile strength of 73 MPa was achieved for the 0° orientation direction (parallel to applied load). 54 MPa was achieved for the 90° orientation perpendicular to the applied load and 66.5 MPa for the alternating 0°/90° configuration [16]. However, considering all the factors contributing to reduced mechanical performance of 3DP objects, the weakest point of the 3DP object is still the sub-optimal adhesion between the layers.

Our study presents in detail how to improve the layer-layer bond for CF/PEEK (carbon fibre PEEK) composites using a modified, inexpensive, commercially available open-source printer, Ultimaker 2+ (UM2+). To the best of our knowledge this work demonstrates the first successful 3D printing of 150CA30 PEEK mould inserts for injection moulding. This allowed our industry partner to produce prototype injection moulded parts (in the hundreds part number range) without the expense of manufacturing an expensive metal insert.

Mechanical performance of the material and parts was studied via tensile testing and dynamic thermomechanical analysis (DMTA). Morphology and crystallinity were measured using XRD, DSC, CT scanning and SEM. The 3DP process was recorded using a thermal imaging camera which showed that a suitably heated chamber is essential to reduce defects in the printed part, especially in the Z direction. The research provides a better understanding of the 3DP of semicrystalline materials where a well-formed crystalline phase is essential to achieve good

thermomechanical properties. Moreover, the results of this work can be applied to other advanced semi-crystalline materials and can also be useful in the optimization of SLS 3DP.

2. Experimental

2.1. Materials

Pellets of VICTREX 150CA30 PEEK containing 30 wt% of short carbon fibre with an average length of 133 mm (± 73 μm) and diameter 6-7 μm were extruded into a filament of diameter 1.75 mm (± 0.10 mm). Before extrusion, the pellets were dried for 24h at 150°C in an oven with air circulation. The filament was dried using the same regime as that for the pellets and then stored in vacuum bags until required for 3DP. The Novodur P2H-AT Acrylonitrile Butadiene Styrene (ABS) and High Impact Polystyrene HI650 (HIPS) used in the injection moulding trials were kindly supplied by Denroy Plastics Ltd.

2.2. Methods

Optical microscopy with rheology were performed using a CSS450 (Linkam) system and Olympus Microscope. Cross-section samples of the 3D printed wall, with a thickness of 100 μm, were cut using a microtome and transferred onto the stage between two glass plates. PEEK crystallite melting dynamics were observed with the optical microscope at a magnification 20x and 50x and in the temperature range from 50 to 400°C at a heating rate of 10°C/min.

X-Ray diffraction (XRD) - measurements were performed using a pinhole camera (MolMet, Rigaku, Japan, modified by SAXSLAB/Xenocs) attached to a microfocused X-ray beam generator (Rigaku MicroMax 003) operating at 50 kV and 0.6 mA (30 W). The camera was equipped with a vacuum version of Pilatus 300K detector. A scattering vector (q) range of 0.2 – 3.6 1/Å was chosen

where $q = \left(\frac{4\pi}{\lambda}\right) \sin\theta$, λ = 1.54 Å is the wavelength of the installed source and 2θ is the scattering angle. Calibration of primary beam position and sample-to-detector distances was performed using a Si powder sample. Homemade software based on PyFAI Python library [17] was used for data reduction. Peak deconvolution was achieved using Fityk software [18].

Transmission electron microscopy (TEM) and *selected area electron diffraction (SAED)* measurements were performed using a field emission Jeol JEM 2100F microscope operated at 200 kV. The samples for TEM analysis were taken from the printed wall and embedded in epoxy resin. This was then microtomed with a diamond knife to obtain slices of 50 nm thickness. Each specimen was transferred to a carbon copper grid and observed in the bright field mode.

Scanning electron microscopy (SEM) with *energy dispersive X-ray (EDX)* analysis was performed using a Hitachi SU5000 field emission instrument equipped with an X-MaxN 80 mm^2 silicon drift detector (Oxford Instruments, UK). An acceleration voltage of 10 KeV was used during imaging. Samples were coated with a thin layer (20 nm) of Au/Pd (60/40 ratio) to make the surface of the samples conductive for electron microscopy. The coating was performed using an Emitech K500X sputtering deposition system with Ar gas plasma.

Dynamic Thermomechanical Analysis (DMTA) was performed using a TA Instruments Q800 DMTA in the dual cantilever mode at 1 Hz and an oscillation amplitude of 15 µm. A heating rate of 10°C/min in the rage of 50 - 330°C. The glass transition temperature, T_g, was taken to be the temperature at the peak of the *Tan* δ curve. The DMTA rectangular specimens were 56 mm in length, 10 mm in width, 3.2 mm in thickness. Three samples were tested for each experiment.

Tensile properties and *flexural properties* were determined using an Instron 5500R Model (Instron Limited, UK) at room temperature and according to the ASTM 638 Type I and ISO 178 Flexural

standards. For each type of processing method and content five specimens were manufactured and tested.

Differential Scanning Calorimetry (DSC) was performed using a TA Q100. The instrument was calibrated with pure indium. 5 mg samples were cut as shown in **SI-Figure 1**. The ramp temperature mode was used with a heating rate of 10°C/min in the rage of 50 - 400°C.

Computerised Tomography (CT-Scans) were obtained using a desktop X-Ray microtomograph SkyScan 1275 with Source Voltage 40 kV and Source Current 250 μA. The Image Pixel Size was equal to 5 μm for filaments (ϕ 1.75 mm) and 8 μm for rectangular (56x10x3.2 mm) specimens.

3. Results and discussion

3.1. Printer modification and printing conditions

An Ultimaker 2+ (UM2+) was modified to enable the printing of CF/PEEK and other high-performance materials. Modifications were achieved using inexpensive and easily sourced components which built on those modifications carried out by other investigators [19]. The main modifications were; the installation of an all-metal hot end capable of reaching temperatures up to 420℃, building a new heated bed with temperature regulation up to 350℃, installation of heating lamps with temperature regulation for the chamber heating up to 230℃ and more. Additionally, thermal insulation was installed to prevent thermal warping of the plastic parts of the printer. The printer with a standard setup was designed for a filament diameter of 2.85 mm. For this diameter, there was a risk of insufficient heat transfer to the filament core at a higher printing speed. That would result in jamming of the extruded material and blockage of the nozzle during the printing process. For this reason, a filament diameter of 1.75 mm was selected to facilitate a printing speed

up to 50 mm/s with a nozzle diameter of 1.2 mm. Finally, modification and calibration of the printer firmware were performed.

The processing parameters are shown in **Table 1**. Different strategies were used in order to determine the influence of chamber temperature on layer-layer adhesion, the effect of post-curing around the glass transition temperature and crystallization behavior on printed part performance. All specimens were printed as solid, fully filled structures.

3.2. Post-curing and build plate temperature

Post curing is often proposed as a method to improve the mechanical properties of a printed part so in this study we have examined post-curing and also looked at how increasing the build plate temperature may be used instead of post-curing. In order to determine the effect of post-curing on the printed part, rectangular ISO 178 samples were printed flat with the build plate at 150℃ and without active heating of the chamber. After that, samples were post-cured in an oven, up to the glass transition temperature for 30 min, then the temperature was increased to 190℃ for 2h and further cooled down to room temperature **SI-Figure 2**. Additionally, samples printed with the build plate set at 240℃ and without active heating of the chamber were printed to assess the effect of build plate temperature on printed part properties. Each sample was cut to a length of 56 mm suitable for DMTA tests and from the remaining piece a 10 mg sample was extracted for DSC.

The shape of the post-cured sample remains the same after the curing procedure and warping was not observed **SI-Figure 3**. The reference specimen printed at 150℃ **Figure 1**, (green lines) has the lowest storage modulus in the glass and rubber region. This is due to the lower crystallinity of this sample which means that chain relaxation is stronger and is visible as the highest *Tan δ* peak [20,21]. Post curing of the sample in the rubber region between the glass transition and melting

point to form secondary crystals should improve the mechanical properties [10,11]. Such post-treatment at 190°C (cold crystallization) increases the crystalline phase which appears as a peak in the DSC at 225°C Figure 1 red line. The physical crosslinks due to the crystal structure reduce the mobility of the chains, observed as a decrease of the *Tan δ* peak for the post-cured specimens [22,23]. When the temperature reaches the melting region of the secondary crystalline phase, around 205°C (purple dash line), it is possible to observe a rapid drop in the mechanical properties between the dashed lines. The storage modulus of the post-cured sample below 205°C is similar to the specimen printed with the build plate at 240°C. The cold crystalline phase is melted around 235°C (dashed black line) and *Tan δ* and the storage modulus revert to a level close to that of the specimen printed at 150°C. Having the building plate temperature at 240°C during 3DP allowed the formation of a well-organized structure without the presence of the secondary crystals peak and only the primary crystalline phase is visible on the DSC curve. The crystalline phase inhibits relaxation of the polymer chain and improves the thermomechanical properties so that the storage modulus in the region above and below the glass transition temperature is the highest (black lines) for this printed part.

For the set of samples printed at 150°C, post-cured at 190°C and printed at 240°C, A comparison of the storage modulus at 100°C, in the glass region, and at 275°C, above vitrification in the rubbery plateau region, confirms the above discussion about the influence of thermal treatment conditions. At 100°C, the sample printed at 150°C, before additional post-curing, has a storage modulus of 6 175 MPa whereas after additional post-curing at 190°C, the modulus increases to 6 767 MPa. Finally, printing with a building plate pre-heated to 240°C favours the formation of a more organized structure, rich in crystalline domains, with a storage modulus of 7 268 MPa. A similar tendency can be observed at 275°C in a rubbery plateau. The sample printed at 150°C was

characterized by a storage modulus of 652 MPa and cold crystallization at 190°C increased the modulus to 694 MPa. Samples printed at 240°C with in situ formation of the crystals reached the highest storage modulus value of 832 MPa.

These investigations clearly show that it is possible to increase the crystalline fraction by cold crystallization during a post cure process. However, printing at a higher build plate temperature achieves better thermo-mechanical performance without the need for a costly and time-consuming post-cure step. This work shows that the crystalline phase is responsible for reversible physical crosslinking which is crucial to attain the highest performance in 3D printed specimens.

3.3. Chamber temperature

In this study a 'wall' of dimensions 120x70x3.4 mm was built at different print chamber temperatures with the build plate temperature maintained at 240°C. The 'wall' structure was chosen because it is representative of the shell and inner wall of the 3D printed injection mould insert that was to be printed in this work **Figure 2 a)**. If this 'wall' structure performance could be optimised then the overall printed insert would be optimised. By changing the current on the lamps, it was possible to vary the chamber temperature between 78°C-230°C. In order to determine the layer-layer adhesion in the wall structure, 5 tensile test samples were cut according to ASTM 638 Type V from the wall using a water-jet cutter. 3 rectangular specimens of dimensions 56x10 mm were cut for DMTA testing and CT scans SI-Figure 1. Samples for DSC and XRD were removed from the top of each wall (since the building plate was heated up to 240°C and the bottom part of the sample would not present representative information). Each layer of the wall was printed by the deposition of 3 strips of molten material along the Y axis. This should lead to a highly anisotropic structure and orientation of the CF short fibres in the Y direction. The temperature of

the chamber was measured using a FLIR E4 Thermal Imaging Camera focused on the middle of the sample during the printing of the last layer.

Figure 2 b) shows how the temperature uniformity of the printed wall improves as the chamber temperature increases with best uniformity being achieved at 230℃. These images also clearly show how the nozzle actively participates in heating up of the top layers. With increasing chamber temperature, it is possible to see that the top layers are warmer, and the range of the top heated region is wider. Heat from the freshly deposited layer at 400℃ is dissipated more slowly at a higher chamber temperature. This should eliminate structural imperfections as the occurrence of coarse pores at the layers' interface and of fine pores at the passes' interface is less likely when the melted polymer is deposited onto a hot surface. Thus, mechanical, thermal and microstructural perfection should improve with increasing chamber temperature.

This can be observed in Figure 2 c) where the tensile strength for printed samples increases from 6.96 MPa when printed at a chamber temperature of 78℃, to 36.28 MPa when printed at a chamber temperature of 230℃, a fivefold increase. Thus, printing with a heated chamber is crucial to achieving good bonding between layers and preventing delamination. Obtained maximum tensile strength of 36.28 MPa is still only 13.5% of the value quoted for injection moulded 150CA30 PEEK which is 270 MPa. However, the 3DP part should not be directly compared with an injection moulded part for a number of reasons. Firstly, during deposition of the filament layers in 3DP the fibres are aligned in the deposition direction (X-Y) so there is no influence of the fibres in the Z direction in which the tensile test is conducted. The Z direction strength is essentially based on that of the unfilled PEEK at the layer interface which depends mostly on the entanglement of the polymer chain at the interface between the layers. Improvement can be achieved only by printing at a chamber temperature sufficiently above the glass transition temperature to allow good chain

mobility and diffusion between layers [6]. Additionally, the strength of the part can be further improved when the crystallinity of the interface layer is maximised. This can only be achieved if the chamber temperature and thus interlayer temperature is kept between T_g and T_m when PEEK chains favourably arrange into strong, well define lamellae. Comparing our results with that for unfilled 150CA30 PEEK (150 PEEK matrix is around 105 MPa) we achieve 34.8% of that strength.

When using an infill pattern of 90º most of the pores formed are located at the junction of two neighboring lines and those defects overlap along the Z-axis and contribute to a reduction of the mechanical properties. Changing the raster angle to an alternating angle of 45º/-45º used in this study should allow more equal distribution of the pores resulting in better properties along the Z axis. The closed porosity of the samples calculated from the micro CT does not exceed 2.3% for printed specimens and is significantly lower than the filament porosity of 6.4% SI-Table 1. The 3D printing process reduces the number of pores observed in the filament by reprocessing the material, which melts the filament in the nozzle and releases trapped air. There is no significant effect of chamber temperature on the closed porosity which fluctuates between 1.0-2.3%.

The positive influence of increasing chamber temperature is also observed in the increasing storage modulus results **Figure 3 a)**. At 100°C DMTA test temperature the sample made at 78°C has a storage modulus of 1 325 MPa whereas the sample printed at a chamber temperature of 230°C has a storage modulus of 2 485 MPa, a difference of 47%. DSC results show that the melting peak (around 343°C) is barely affected by (about 1°C) the chamber temperature Figure 3 b). Secondary crystals start to melt above the glass transition temperature and their melting point increases with their thickness. It can be observed that with increasing chamber temperature the secondary melting point is shifted to higher temperatures. The secondary crystals start to melt around 280°C and

225℃ respectively for specimens printed at 230℃ and 180℃ (visible as a gentle slope in the heat flow curves marked by arrows, Figure 3 b).

Published crystallinity versus chamber temperature for neat 450G PEEK report that between 100℃ and 200℃ there are no significant changes, being respectively 29% and 31% [12]. Our results are slightly higher. With the building plate set on 240℃ the chamber heated up to 78℃ and that was sufficient to obtain a crystallinity of around 33.4%, DSC crystallinity **Table 2**. The higher degree of crystallinity may be due to the carbon fibre acting as a nucleation agent. Increasing the chamber temperature results in a corresponding increase in crystallinity, from 33.4% to 38.9% in going from 78℃ to 230℃. The crystallinity determined via XRD has much higher values than that calculated from DSC. In the case of the XRD, the calculation shows total crystallinity as a sum of primary and secondary crystals whereas for the DSC technique the crystallinity was calculated from the primary crystal melting peak. The size of the crystal determined by XRD was around 7 nm and is not affected by chamber conditions.

This study shows clearly how increasing chamber temperature increases the fraction of primary crystals in the printed part. Attaining a high level of primary crystallinity is critically important for the structural properties of the printed part, particularly if it is to be used as a tooling insert for injection moulding where it will experience repeated high temperatures and pressures during the injection moulding process. Only thick and large lamellae can maintain the integrity of the 3D printed mould insert at elevated temperatures where weak and thinner low-temperature secondary crystals would be melted Figure 1. Black vs Red lines.

The flexural properties for specimens printed flat on a building plate set at 240℃, with and without a heated chamber (at 230℃), indicate that having the chamber heated to 230℃ increases the flexural modulus from 10 810 MPa to 14 946 MPa, an improvement of 27.7% **SI-Table 2**. The

flexural stress at break similarly increased by around 18.6% from 202.6 to 248.9 MPa for the part printed with the heated chamber. The flexural stress at break and modulus of injected moulded samples, according to the producer data sheets, are respectively 380 MPa and 24 000 MPa. Even though our flexural stress at break and modulus results are thus 34.5% and 37.7% lower than those for injection moulded parts they are, to the authors best knowledge, the highest, so far published results for 3D printed PEEK materials **SI-Table 3** [6,7,12,14-16,24,25]. Our tensile modulus is also the highest published to date, being 77% higher than that reported for SLS CF/PEEK [24].

A comparison between 3D printed and injection moulded tensile specimens shows that stress at break and modulus were respectively 59.0% and 45.8% lower for the 3DP parts. Such large differences between 3D printed and injection moulded samples are a result of the non-continuous character of 3D printed parts in the Z-direction, the alignment of the fibre orientation according to the movement of the printer head and to voids generated during printing. These imperfections are common for all polymers used in the FFF 3DP process.

3.4. Carbon fibre orientation

The orientation of the discontinuous carbon fibres in the 3D printed object has a strong influence on the storage modulus. A comparison of a sample printed as a wall and printed as a flat part shows that storage modulus at 100°C is 2 485 MPa and 7 268 MPa respectively Figure 3 c). During dual cantilever measurements, stress act parallel to the deposited layers and modulus represents the bond strength of the layers. Moreover, that value is in close agreement with the storage modulus of the unfilled PEEK material [5] and supports the concept that tensile properties between the layers are dominated by the matrix rather than the composite properties. For specimens printed in a flat orientation, stress is applied perpendicularly to the layers and fibres during the DMTA test.

Thus, higher storage modulus is observed at all temperatures. The slight increases of the storage modulus above 220℃ Figure 3 c) - the red line is related to the fibre reorganization after reaching the melting point of the PEEK crystalline fraction Figure 3 b) - Pink arrow. Fibres act as a nucleation agent and are surrounded by PEEK crystals. As long as the melting point of those crystallites is not reached, carbon fibres cannot change their orientation. Thanks to the mutual synergy of the carbon fibre locked into the PEEK crystallites, it is possible to observe an improvement of the storage modulus. After melting of the crystalline structure, small movement and reorientation of fibres is possible. Thus, both specimens represent similar storage modulus values around the melting point when fibres flow randomly in the polymer melt.

3.5. Morphology

The morphology of the 3DP walls was examined using an optical microscope with a hot stage and polarizers as well as by SEM. Samples for optical microscopy were cut with a thickness of 100 microns. It is possible to notice that the heated chamber enables the formation of a structure richer in well-formed crystallites, **Figure 4** - Upper row. Moreover, deposited layers cool down more slowly which helps in the formation of a more continuous structure surrounding the carbon fibres. The presence of the carbon fibre is not so evident for the sample printed at 78℃ compared with that printed at a chamber temperature of 230℃ due to larger amorphous phase. The half-time of PEEK crystallization reaches a minimum around 230℃ and that seems to be the optimal temperature for the 3DP process for PEEK [11]. Results for the 78℃ chamber are less continuous and the crystalline domains are less well defined, with limited tendency for mutual interpenetration.

The crystalline structure is stable over the wide range of temperatures examined with no significant differences up to 300℃ **SI-Figure 4**. Above that temperature, it is possible to notice an increase

in the brightness which suggests partial melting of the weaker and thinner secondary crystallites which start to melt around 280℃ according to the DSC thermograms. Further increase of the temperature leads to melting of the PEEK crystals at a melting temperature around 343℃ and at 360℃ they are turned in the isotropic liquid with random molecular ordering.

Crystallite domains are significantly larger for the specimen printed with a high chamber temperature and have an ellipsoidal shape Figure 4 – Middle row. Flattening is visible in the Z direction. Most of the domains do not exceed a diameter of 100 μm. However, several of them reach a diameter in the Z direction above 150 μm for the specimen printed at 230℃. It appears that domains are formed by agglomerated carbon fibres covered by PEEK crystallites. That is important because layer thickens during printing was set for 100 μm and it is visible as darker straight lines, so most of the domains are created in the region of the single layer and do not take part in reinforcement between the layers. For the specimen printed at 78 ℃ the size of the domains does not exceed 100 μm which also explains why properties in the Z direction are so weak for the CF/PEEK composite printed at this condition. Three main factors contribute to this. Firstly, CFs are aligned according to the movement of the printing head and filler cannot effectively join two layers because is aligned horizontally rather than vertically. This is clearly visible by SEM SI-Figure 5. The second reason is that large crystallites are formed in the single layer, printed with height 100 μm and crystallisation is not dominant at the junction of layers. Thus, the crystalline phase has a noncontinuous character and mechanical properties are weaker in the Z direction. Only printing with a chamber at a high temperature allows the crystalline domains to achieve a size that exceeds the layer thickness. Additionally, PEEK crystals formed at the top of the layer need to be melted to bond properly with the newly deposited layer. When the chamber is not sufficiently heated, there is not enough energy to melt the crystals in the already deposited layer. For a chamber

heated to 230°C, the new layer is much better infused in the previous one and the crystal domains formed during cooling reach a thickness in the Z direction above 100 µm. The layers are therefore well connected by the crystalline PEEK domains thus explaining the more the 5-times better mechanical properties in the Z direction for parts printed at the high chamber temperature.

The diameter of the carbon fibre in the CF/PEEK was evaluated by polarised microscopy at around 6-7 µm. Longitudinal crystals covering the carbon fibre are noticeable on CT scans as more dense yellow regions with a length of around 80-100 µm and a diameter between 8-11 µm Figure 4 – Bottom row. As stated earlier, the carbon fibre acts as a nucleation agent and growing crystals enrobe the carbon fibre slightly increasing its diameter (from 6-7 µm to 8-11 µm). Also, it is possible to observe spheres with a diameter of between 23-63 µm. Smaller objects cannot be detected by this technique because the pixel size is equal to 8 µm in the case of the rectangular specimens compared with pixel size 5 µm when the filament was scanned. This is due to the different distances between object and source. In the case of more bulk rectangular specimens with a width of 10 mm it was necessary to increase the distance from the source to avoid contact with it.Spherulitic crystalline structures are very well-formed at all chamber temperatures examined as can be seen in Figure 5. It appears that the thermo-dissipative character of the CF filler partially arrests the formation of the spherulites, visible close to the carbon fibre on the amorphous region of the PEEK **Figure 5 a) – c)**. This figure also shows how the crystalline structures initially form and then grow into well-formed spherulites [26].

Spherulites seem to be well interconnected and create a well-defined physical network with areas of amorphous material. A comparison of samples Figure 5 d) and e) clearly indicates that the part printed at the highest chamber temperature has a thicker lamellar structure and the spherulites are well interlocked, **SI-Figure 5**. The size of the single spherulite are not change significantly with

increasing chamber temperature and the highest density is noticed around the carbon fibres. This supports the results from the polarised microscopy and CT-scans. The lamellar thickness of the spherulites rises from 25 nm for the 78 ℃ chamber to 50 nm when chamber was at 230℃. Measurement were taken for lamellae with approximately the same distance from the core of the spherulite. This clearly explains why mechanical properties are improved for samples printed at the higher chamber temperature.

3.6. Crystallinity

The TEM images of the CF/PEEK samples, show the carbon fibre filler and the PEEK matrix Figure 6 a) and b). Figure 6 b) is a magnified image of the yellow square in Figure 6 a). Magnification shows the PEEK crystalline regions with (200) plane and CF, indicating the crystalline nature of PEEK and non-crystalline nature of CF. The high-resolution TEM image depicts the lattice spacings corresponding to the PEEK (003) plane Figure 6 c). On the inset, it is possible to observe the corresponding SAED pattern indicating the various planes for an orthorhombic PEEK crystal [27,28]. The spacings in the reciprocal lattice corresponds to 0.47 nm, 0.33 nm and 0.27 nm interplanar spacings. These interplanar spacings correspond to the (110), (003) and (111) planes, respectively as marked in the inset Figure 6 c).

XRD analysis of the wall for different chamber temperatures is shown in Figure 6 d). Specifically, peaks at 18.9°, 20.8°, 22.7°, 26.4° and 28.7° are attributed to the orthorhombic PEEK crystal planes (110), (111), (200), (003) and (211), respectively. This plot was also used to calculate crystallinity values **SI-Eq (1)** and crystal grain size from the Scherrer equation **SI-Eq (2)**, values are shown in Table 2.

3.7. Injection moulding trials with a 3DP PEEK tooling insert

A mould insert for injection moulding trials was 3D printed using 150CA30 CF/PEEK with the chamber pre-heated to 230°C, nozzle temperature set to 400°C, printing speed set at 40 mm/s, a nozzle size of 1.2 mm and a layer thickness 0.1 mm.. This was printed as a solid part to enable it to withstand the high injection pressures and temperatures in the mould during injection of molten polymer into the mould **Figure 7 a)** and **b)**.

Fifty shots of HIPS were injected followed by another fifty shots of ABS to produce parts like those shown in Figure 7 c). For both the HIPS and the ABS the melt temperature was above the glass transition temperature, 169°C, of the 150CA30 CF/PEEK but in each case the insert maintained its mechanical integrity and the injection moulded parts had the correct dimensions, SI-Table 4. Deformation of the mould or creep behaviour was not observed. This is due to the immobilization of the amorphous phase by a high content of short carbon fibre and the well-formed crystalline structure of the CF/PEEK insert.

4. Conclusion

This work has shown that CF/PEEK (150CA30 PEEK) can be successfully used to manufacture mold inserts, via FFF 3DP, for the injection molding of commodity plastics and can be an excellent replacement for the commonly used aluminum inserts which are too expensive for low to middle-scale production or prototyping. The “wall” structure allowed a precise study of the bonding between layers in 3D printed objects especially when the strength of a shell structure must be determined. Primary crystals are responsible for the thermal stability of the printed part, the thickness of the lamellae increasing with increasing chamber temperature. Increasing the chamber temperature transforms the secondary crystals into stronger and thicker lamellae with diameter

rising from 25 nm to 50 nm which leads to an increase in mechanical properties both in the glass and rubber regions. Tensile strength was increased more than fivefold from 6.96 MPa to 36.28 MPa for a chamber temperature increase from 78°C and 230°C. Spherulite diameter is unchanged with higher chamber temperature but the thickness of the branches is larger and that directly corresponds to the mechanical properties. The short carbon fibre filler acts as a nucleation agent and is covered in PEEK spherulites. High chamber temperatures allow a reduction in the stress acting on the freshly deposited layer and increases the mechanical properties for a number of reasons: The previously deposited layer is at a higher temperature that allows better bonding with the newly deposited layer and shrinkage and warpage of the part are reduced by keeping the 3DP part at a high temperature throughout the printing process.

Acknowledgement

The authors would like to thank Invest Northern Ireland for funding of the Competence Centre project entitled *Rapid tooling for injection moulding and composite lay-up.*

Supporting Information

Supplementary data associated with this article can be found in the online version.

References

1. Ueda, M., Kishimoto S, Yamawaki, M., Matsuzaki, R., Todoroki, A., Hirano, Y., Le Duigou A. 3D compaction printing of a continuous carbon fiber reinforced thermoplastic, *Composites Part A*, **2020**, 137, 105985
2. Palmero, E.M., Casaleiz, D., de Vicente, J., Hernández-Vicen, J., López-Vidal, S., Ramiro, E., Bollero, A., Composites based on metallic particles and tuned filling factor for 3D-printing by Fused Deposition Modeling, *Composites Part A*, **2019**, 124, 105497
3. Bodaghi, M., Ban, D., Mobin, M., Park, C.H., Lomov, S.V., Nikzad, M., Additively manufactured three dimensional reference porous media for the calibration of permeability measurement set-ups, *Composites Part A*, **2019**, 139, 106119

4. Liu D., Fu J., Fan H., Li D., Dong E., Xiao X., Wang L., Guo Z., Application of 3D-printed PEEK scapula prosthesis in the treatment of scapular benign fibrous histiocytoma: A case report, *J. Bone. Oncol.* **2018**, 12, 78-82
5. Berretta S., Evans K., Ghita O., Additive manufacture of PEEK cranial implants: Manufacturing considerations versus accuracy and mechanical performance *Mater. Des.* **2018**, 139, 141-152
6. Berretta S., Evans K., Ghita O., Processability of PEEK, a new polymer for High Temperature Laser Sintering (HT-LS), *Eur. Polym. J.* **2015**, 68, 243-266
7. Rinaldia M., Ghidinic T., Cecchinia F., Brandaoc A., Nannia F., Additive layer manufacturing of poly (ether ether ketone) via FDM, *Composites Part B*, **2018**, 145, 162–172
8. Stepashkin A.A., Chukov D.I., Senatov F.S., Salimon A.I., Korsunsky A.M., Kaloshkin S.D., 3D-printed PEEK-carbon fiber (CF) composites: Structure and thermal properties, *Compos. Sci. Technol.* **2018**, 164, 319-326
9. Luo, M., Tian, X., Shang, J., Yun, J., Zhu W., Li, D., Qin, Y. Bi-scale interfacial bond behaviors of CCF/PEEK composites by plasma-laser cooperatively assisted 3D printing process, *Composites Part A*, **2020**, 131, 105812
10. Tan S., Su A., Luo J., Zhou E., Crystallization kinetics of poly(ether ether ketone) (PEEK) from its metastable melt *Polymer*, **1999**, 40, 1223-1231
11. Tardif X., Pignon B., Boyard N., Schmelzer J. W.P., Sobotka V., Delaunay D., Schick C., Experimental study of crystallization of PolyEtherEtherKetone (PEEK) over a large temperature range using a nano-calorimeter *Polym. Test.* **2014**, 36, 10-19
12. Yang C., Tian X., Li D., Cao Y., Zhao F., Shi C., Influence of thermal processing conditions in 3D printing on the crystallinity and mechanical properties of PEEK material *J. Mater. Process. Manuf. Sci.* **2017**, 248, 1-7
13. Jonas A. M., Russell T. P., Yoon D. Y., Synchrotron X-ray Scattering Studies of Crystallization of Poly(ether-ether-ketone) from the Glass and Structural Changes during Subsequent Heating-Cooling Processes *Macromolecules*, **1995**, 28, 8491-8503
14. Wu W., Geng P., Li G., Zhao D., Zhang H., Zhao J., Influence of Layer Thickness and Raster Angle on the Mechanical Properties of 3D-Printed PEEK and a Comparative Mechanical Study between PEEK and ABS *Materials* **2015**, 8, 5834-5846
15. Deng X., Zeng Z., Peng B., Yan S., Ke W., Mechanical Properties Optimization of Poly-Ether-Ether-Ketone via Fused Deposition Modeling, *Materials*, **2018**, 11, 216-227.
16. Rahman K. M., Letcher T., Reese R., Mechanical Properties of Additively Manufactured PEEK Components Using Fused Filament Fabrication, *Conference Paper ASME*, **2015**, 2A, 13-19
17. Kieffer J., Karkoulis D., PyFAI, a versatile library for azimuthal regrouping, *J. Phys.: Conf. Ser.* **2013**, 425, 202012
18. Wojdyr M., Fityk: a general-purpose peak fitting program, *J. Appl. Cryst.* **2010**, 43, 1126-1128
19. Turning a desktop 3D printer into a high temperature printer for PEEK AND PEI, available from: https://www.3d4makers.com/blogs/news/turning-a-desktop-3d-printer-into-a-high-temperature-printer, accessed on 15-09-2020.
20. Rodzeń K., Strachota A., Raus V., Pavlova E., Behavior of Tin-Based "Super-POSS" Incorporated in Different Bonding Situations in Hybrid Epoxy Resins, *Polym. Degrad. Stab.,* 2017, 142, Pages 1-20

21. Strachota A., Rodzeń K., Raus V., Ribot F., Janata M., Pavlova E., Incorporation and chemical effect of Sn-POSS cages in poly(ethyl methacrylate) *European Polymer Journal*, **2015**, 68, 366-378
22. Strachota B., Strachota A., Horodecka S., Steinhart M., Kovářová J., Pavlova E., Ribot F., Polyurethane nanocomposites containing the chemically active inorganic Sn-POSS cages, *Reactive and Functional Polymer*s, 2019, 143, 104338
23. Golbang A., Harkin-Jones E., Wegrzyn M., Campbell G., Archer E., McIlhagger A., Production and characterization of PEEK/IF-WS2 nanocomposites for Additive Manufacturing: simultaneous improvement in processing characteristics and material properties, *Additive Manufacturing*, **2020**, 31, 100920
24. Mengxue Y., Xiaoyong T., Gang P., Dichen L., Xiaoyu Z. High temperature rheological behavior and sintering kinetics of CF/PEEK composites during selective laser sintering, *Composites Science and Technology*, **2018**, 165, 140–147
25. Berretta S., Davies R., Shyng Y.T., Wang Y., Ghita O., Fused Deposition Modelling of high temperature polymers: Exploring CNT PEEK composites, *Polymer Testing*, **2017**, 63, 251-262
26. Wang Y., Beard J. D., Evans K. E., Ghita O., Unusual crystalline morphology of Poly Aryl Ether Ketones (PAEKs) *RSC Adv*., **2016**, 6, 3198
27. Wang Y., Chen B., Evans K., Ghita O., Enhanced Ductility of PEEK thin film with self-assembled fibre-like crystals, *Nature*, **2018**, 8, 1-13
28. Wang S., Wang J., Liu T., Mo Z., Zhang H., Yang D., Wu Z., The crystal structure and drawing-induced polymorphism in poly(aryl ether ketone)s, 2: Poly(ether ether ketone ketone), PEEKK, *Macromol. Chem. Phys.*, **1997**, 198, 969-982.

Figure 1 Study of the effect of 3D printing conditions on the thermomechanical properties of 3DP parts (print temperature refers to the build plate temperature).

Figure 2 a) Mold for injection molding generated by Cura 3.6 showing different regions of 3D printed part, b) Heat distribution in the samples for different chamber temperatures detected just as the printing process finished and c) Tensile Strength versus chamber temperature.

Figure 3 Effect of chamber temperature on a) Storage modulus, b) DSC at a building plate temperature of 240°C and c) DMTA for samples printed in wall or flat orientation for two chamber

temperatures. The lines represent sample: cut out from the "wall" structure ZY - red and printed flat in XY orientation as single - black.

Figure 4 Upper row - samples cut from the middle of the 3D printed wall. Measured at ambient condition with objective 20x by polarisation microscope. Middle - row CT Scans of 3D printed samples with pixel size 8 μm, left side samples printed at chamber temperature 230℃ and right-side sample printed at 78℃ respectively. Lower row – CT Scans of the extruded filament with pixel size 5 μm, left side inset.

Figure 5 Top layer SEM images of the flexural samples printed as flat a) - d) temperature of chamber 78℃, e) sample printed with chamber temperature 230℃.

Figure 6 TEM image of a) CF/PEEK and b) zoomed in image. c) HRTEM of PEEK in CF/PEEK, c) sample showing the lattice fringes with inset shows the corresponding SAED pattern and d) XRD for samples printed at chamber temperatures of 78°C, 110°C and 230°C.

Figure 7 Mould used during injection moulding process: a) CAD design, b) 3D printed version with 150CA30 PEEK and c) randomly selected injection moulded parts in black ABS (left) and white HIPS (right).

Table 1 Printing conditions for specimens printed as a wall structure and a flat structure on the building plate

Printing parameters			Chamber temperature for		
	Description	Value		Current on the lamps [A]	Temperature [℃]
	Nozzle diameter	1.2 mm		0	78
	Layer Thickness	0.1 mm		1	80
	Nozzle temperature	400℃		1.5	110
	Building plate temperature	240℃		2	140

Printing speed	40 mm/s	2.5	180
Raster angle	Wall structure ZY 90º Other Specimens XY 45º/-45º	3	230

Table 2 Chamber temperature for wall structure versus crystallinity calculated from DSC, SI (1) and XRD, SI (2).

Chamber Temperature [°C]	ΔH_c [W/g]	X_c^{DSC} [%]	X_c^{*DSC} [%]	X^{XRD} [%]	*Grain size* [nm]
78	33.46	25.7	33.4	41.5	6.93
80	35.32	27.1	35.3	-	-
110	35.80	27.5	35.8	47.4	7.18
140	37.15	28.6	35.8	-	-
180	37.97	29.2	38.0	-	-
230	38.76	29.8	38.9	48.7	7.08

Heat flow ΔH_c [W/g], X_c^{DSC} crystallinity fraction calculated from DSC, X_c^{*DSC} crystallinity fraction calculated from DSC with excluded filler weight fraction, Xc^{*XRD} crystallinity fraction calculated from XRD with excluded filler weight fraction, Average *Grain size* [nm].

Figure 1

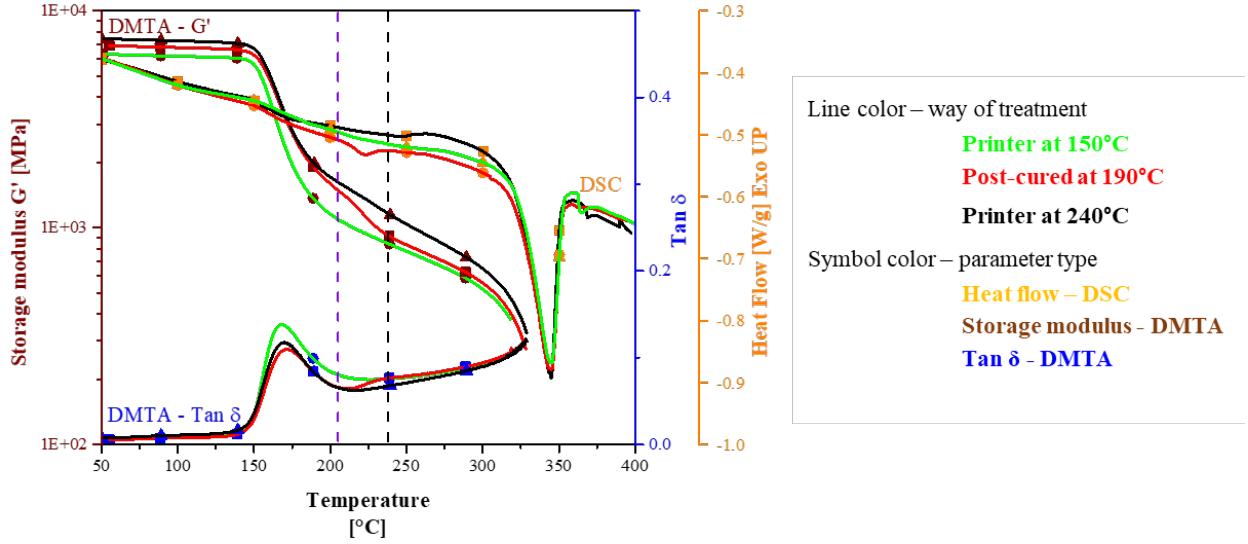

Figure 2

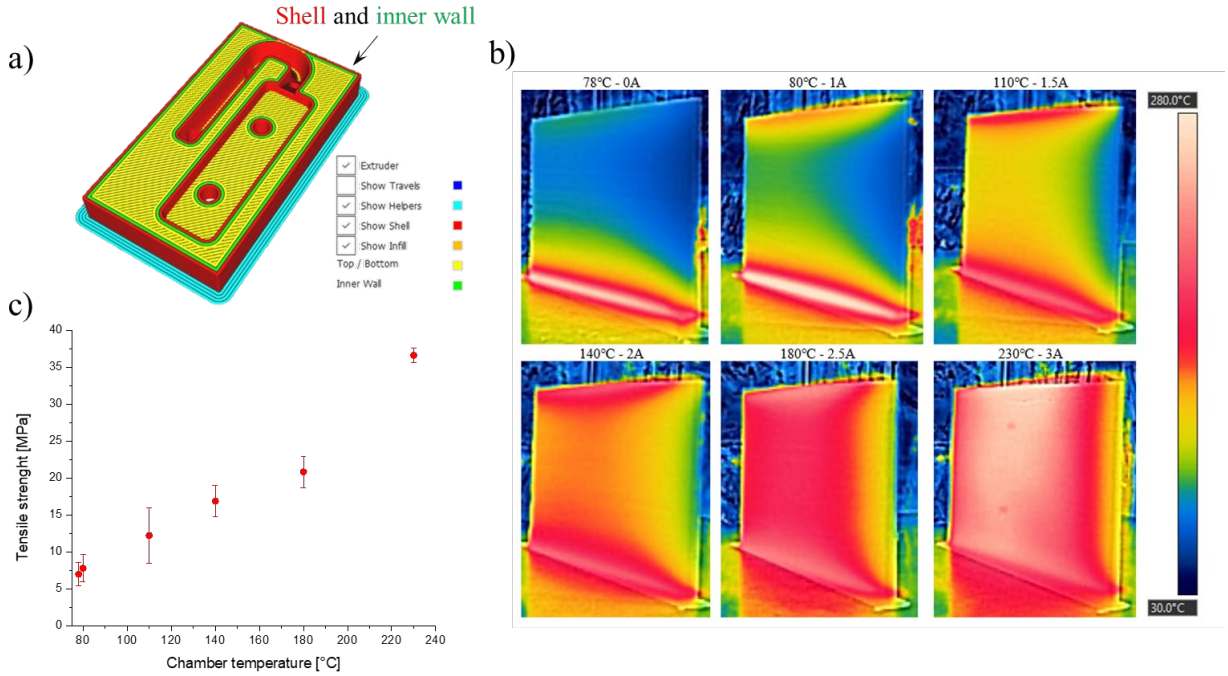
a)
Shell and inner wall
Extruder
Show Travels
Show Helpers
Show Shell
Show Infill
Top / Bottom
Inner Wall
b)
78°C - 0A
80°C - 1A
110°C - 1.5A
140°C - 2A
180°C - 2.5A
230°C - 3A
280.0°C
30.0°C
c)
Tensile strenght [MPa]
Chamber temperature [°C]
0
5
10
15
20
25
30
35
40
80
100
120
140
160
180
200
220
240

Figure 3

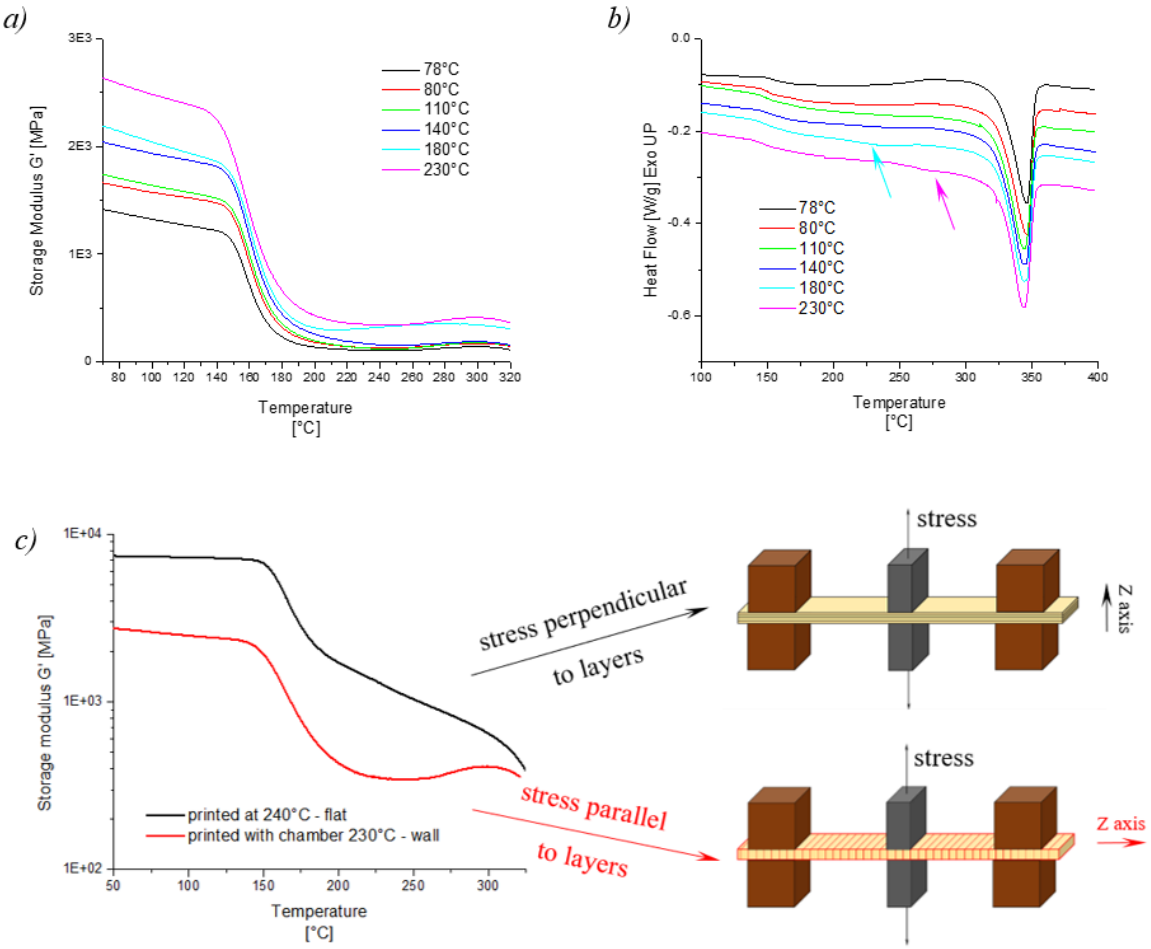

Figure 4

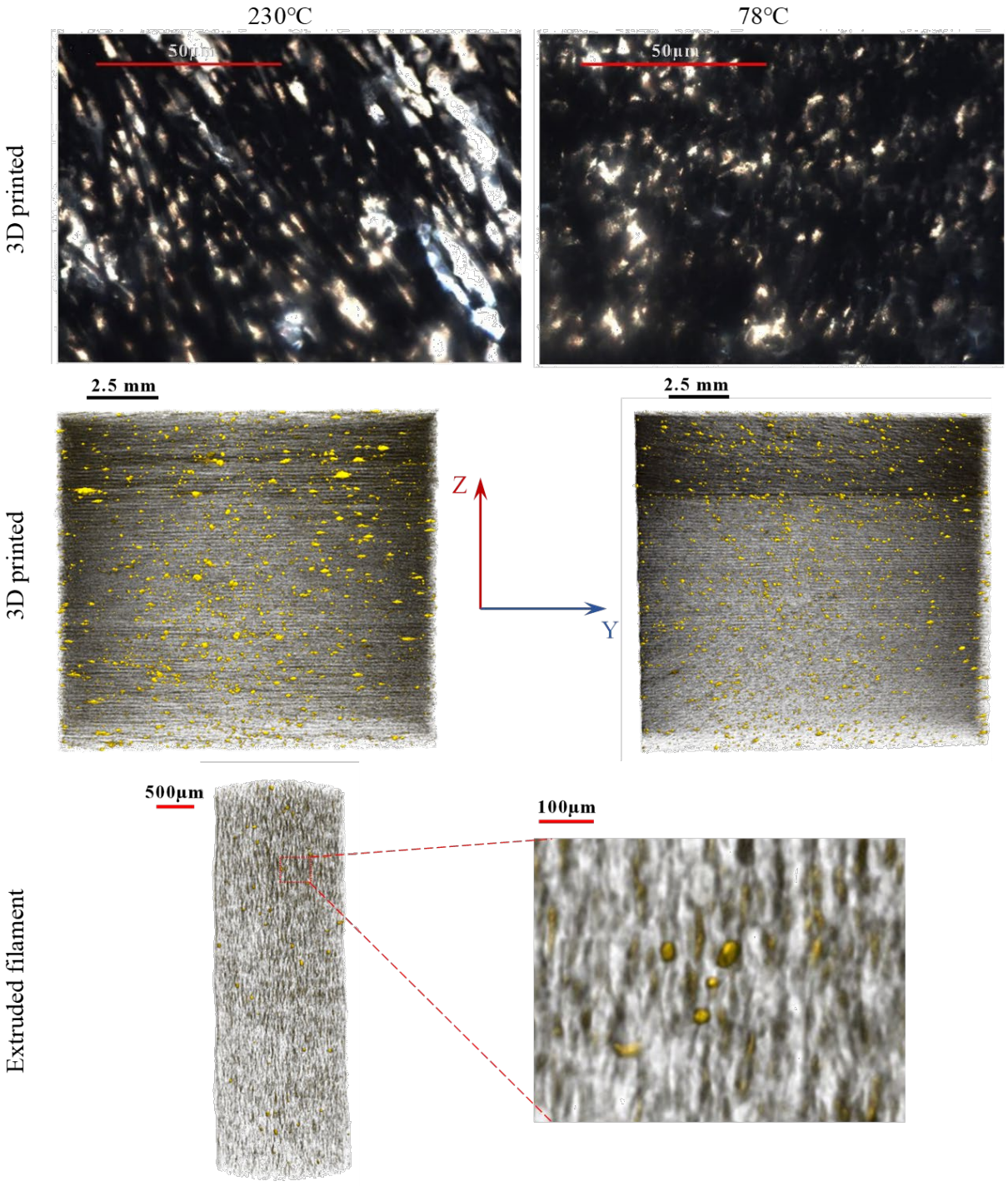
230°C
78°C
50µm
50µm
3D printed
2.5 mm
2.5 mm
Z
Y
3D printed
500µm
100µm
Extruded filament

Figure 5

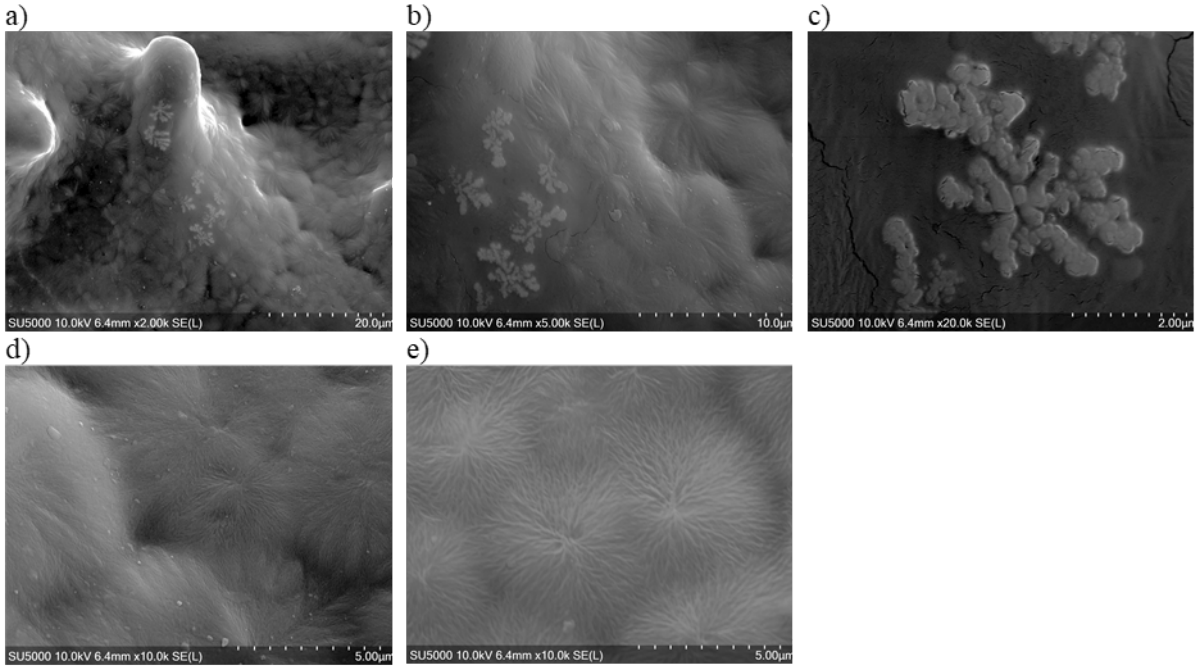
a)
SU5000 10.0kV 6.4mm x2.00k SE(L)
20.0µm
b)
SU5000 10.0kV 6.4mm x5.00k SE(L)
10.0µm
c)
SU5000 10.0kV 6.4mm x20.0k SE(L)
2.00µm
d)
SU5000 10.0kV 6.4mm x10.0k SE(L)
5.00µm
e)
SU5000 10.0kV 6.4mm x10.0k SE(L)
5.00µm

Figure 6

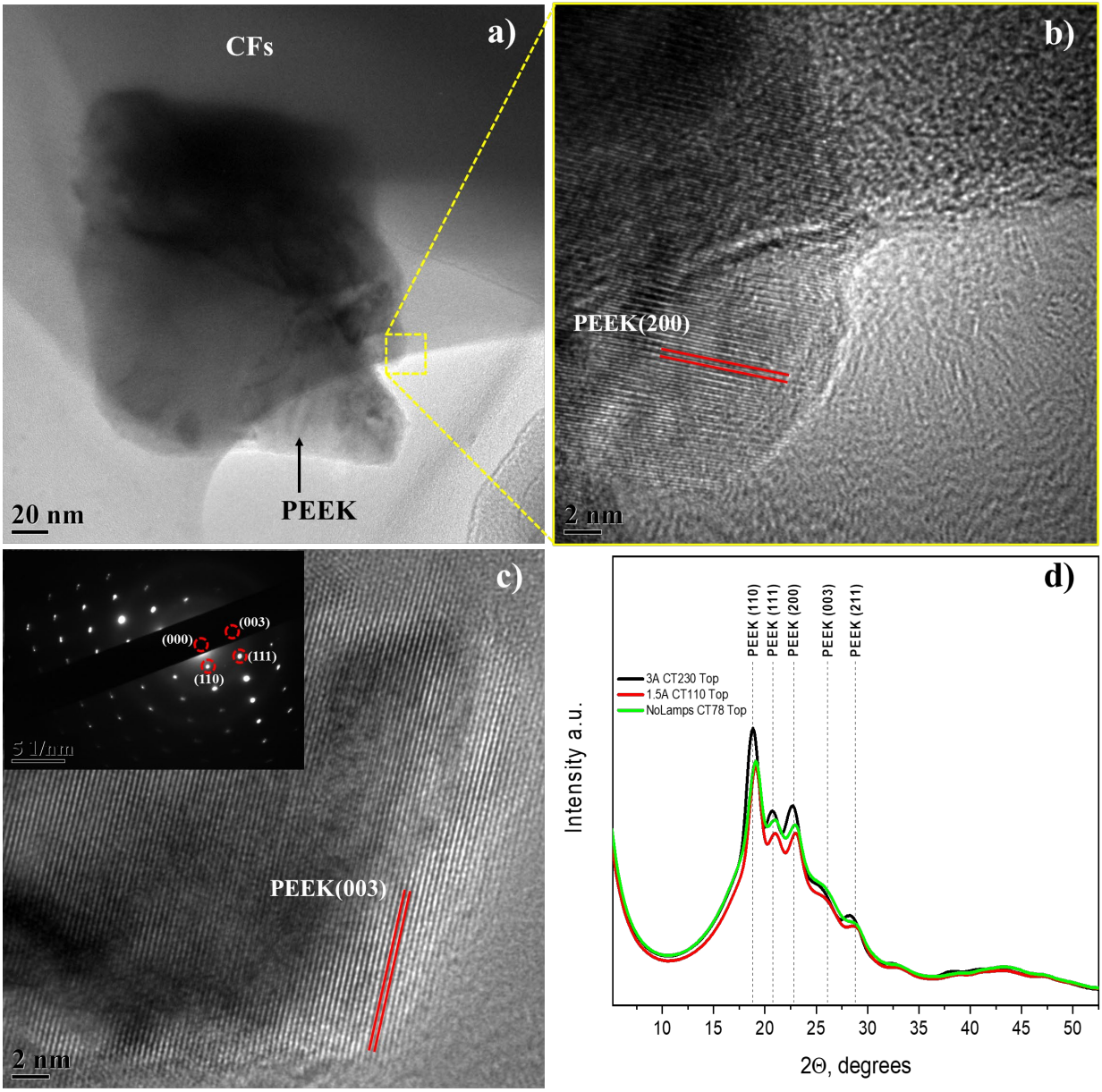
a)
CFs
20 nm
PEEK
b)
PEEK(200)
2 nm
c)
(003)
(000)
(111)
(110)
5 1/nm
PEEK(003)
2 nm
d)
PEEK (110)
PEEK (111)
PEEK (200)
PEEK (003)
PEEK (211)
3A CT230 Top
1.5A CT110 Top
NoLamps CT78 Top
Intensity a.u.
10
15
20
25
30
35
40
45
50
2Θ, degrees

Figure 7